Research Square

Preprints are preliminary reports that have not undergone peer review.
They should not be considered conclusive, used to inform clinical practice,
or referenced by the media as validated information.

Collateral vessel density modulates arteriovenous malformation severity

Hyunwoo Choi
Barrow Neurological Institute
Han Kyu Lee
Duke University School of Medicine
Douglas A. Marchuk
Duke University School of Medicine
S. Paul Oh
ohp@barrowneuro.org

Barrow Neurological Institute

Short Report

Keywords:

Posted Date: November 18th, 2026

DOI: https://doi.org/10.21203/rs.3.rs-11578259/v1

License: This work is licensed under a Creative Commons Attribution 4.0 International License.
Read Full License

Additional Declarations: No competing interests reported.

Collateral vessel density modulates arteriovenous malformation severity

Hyunwoo Choi, PhD[1]; Han Kyu Lee, PhD[2], Douglas A. Marchuk, PhD[2], S. Paul Oh, PhD[1,3]

1. Barrow Aneurysm & AVM Research Center, Department of Translational Neuroscience, Barrow Neurological Institute, Phoenix, AZ 85013, USA
2. Department of Molecular Genetics and Microbiology, Duke University School of Medicine, Durham, NC 27710, USA
3. Lee Gil Ya Cancer and Diabetes Institute, Gachon University, Incheon, Republic of Korea

Running Title: Collateral density modulates AVM severity

Correspondence:
S. Paul Oh, Ph.D.
Barrow Aneurysm and AVM Research Center
Department of Translational Neuroscience,
Barrow Neurological Institute
350 W Thomas Road
Phoenix, AZ 85013
E-mail: ohp@barrowneuro.org
Phone and fax numbers: +1-602-406-3732 (phone), +1-602-406-4172 (FAX)

Abstract

Arteriovenous malformations (AVMs) are high-flow vascular anomalies defined by direct artery-to-vein shunts, often resulting in hemodynamic instability, vessel rupture, and life-threatening hemorrhage. Causative mutations in *ENG, ALK1, and SMAD4* are well-established in hereditary hemorrhagic telangiectasia (HHT), yet AVM severity varies widely among individuals carrying the same mutation, implicating host-specific modifiers that remain poorly defined. Here we test whether collateral vessel density modifies AVM severity *in vivo*. Using *Rabep2*-knockout mice, which have reduced collateral vessel density, we examined AVM severity in two independent AVM mouse models (*Eng*- and *Alk1*-inducible knockouts). *Rabep2* deletion significantly reduced the number of pial and dorsal skin collaterals; this was accompanied by attenuated AVM formation, with smaller lesion volume and preserved hemoglobin levels. Collateral number correlated positively AVM severity at the individual animal level. In a retinal AVM model lacking native collaterals, *Rabep2* deletion did not alter AVM formation, indicating that this effect requires a collateral network. These results identify collateral vessel density as a physiological modulator of AVM severity and suggest that vascular architecture and hemodynamics, rather than genetic signaling alone, shape AVM outcome.

Keywords: AVM severity, collateral density, *Rabep2*, Hereditary hemorrhagic telangiectasia

Non-standard Abbreviations and Acronyms: AVM, arteriovenous malformation; AVF, arteriovenous fistula; AV, arteriovenous; iKO, inducible knockout; dKO, double knockout; P, postnatal day; bw, body weight

Introduction

Arteriovenous malformations (AVMs) are high-flow vascular shunts between arteries and veins that bypass the capillary bed, leading to hemorrhage and tissue injury. Hereditary hemorrhagic telangiectasia (HHT), an autosomal dominant vascular disorder caused by mutations in *ENG, ALK1* and *SMAD4*, is characterized by mucocutaneous telangiectases and AVMs in the lung, liver, brain, and gastrointestinal tract. Lesion severity, however, varies widely among individuals carrying identical mutations, implicating additional host-specific modifiers.

Collateral circulation consists of collateral arteries (artery-to-artery anastomoses) and microvascular collaterals (arteriole-to-arteriole anastomoses), and redistributes blood flow and buffers pressure gradients under hemodynamic stress [1]. This network limits ischemic injury during vascular obstruction by maintaining compensatory blood flow [2–4]. Collateral density and diameter in the heart, brain, and limbs vary considerably among individuals, and patients with a well-developed network can remain asymptomatic despite obstruction [1, 5]. Mouse brain pial collaterals form an adaptive network exhibiting strain-specific variability in density and diameter [1, 6]. Rab GTPase-binding effector protein 2 (RABEP2) determines native collateral density and also regulates VEGFR2 trafficking in endothelial cells [7–9]. Because *Rabep2* loss markedly reduces collateral density without overtly impairing developmental angiogenesis [8], *Rabep2*-knockout mice allow the contribution of the collateral networks to AVM development to be tested directly.

We hypothesized that collateral vessel density acts as a hemodynamic amplifier of AVM severity: abundant collaterals would increase inflow and flow convergence within pathological shunts, whereas sparse collateralization would limit lesion progression.

Materials and Methods

Mice

Rosa26$^{CreER/+}$ (R26$^{CreER/+}$; JAX stock #008463) and *Scl*CreER lines were used for global and endothelial cell-specific gene deletion, respectively [10, 11]. The generation of *Alk1*$^{2loxp(2f)}$ and *Eng*$^{2loxp(2f)}$ alleles was previously described [12, 13]. *Rabep2*-knockout mice (*Rabep2*-KO, *Rabep2*$^{-/-}$) in the C57BL/6J background were provided by Dr. D. Marchuk [8]. All comparisons were made between littermates obtained from heterozygous crosses: R26$^{CreER/+}$;*Alk1*$^{2f/2f}$;*Rabep2*$^{+/-}$ and *Alk1*$^{2f/2f}$;*Rabep2*$^{+/-}$, *Scl*CreER;*Eng*$^{2f/2f}$;*Rabep2*$^{+/-}$ and *Eng*$^{2f/2f}$;*Rabep2*$^{+/-}$, or *Scl*CreER;*Alk1*$^{2f/2f}$;*Rabep2*$^{+/-}$ and *Alk1*$^{2f/2f}$;*Rabep2*$^{+/-}$.

For Cre-mediated deletion of conditional alleles, tamoxifen was administered as follows. In the wound-induced AVM model using R26$^{CreER/+}$;*Alk1*$^{2f/2f}$ (*Alk1*-inducible knockout, *Alk1*-iKO) mice, tamoxifen (100 μg/g body weight (bw), dissolved in corn oil; Sigma, C8267) was injected intraperitoneally once on the day of wounding (Day 0) in adult males and females. For brain AVM analysis in endothelial-specific *Eng*-iKO (*Scl*CreER;*Eng*$^{2f/2f}$; *Eng*-iKO^{EC}) mice, tamoxifen (25 μg/g bw) was administered intragastrically for three consecutive days at postnatal day (P)1, P2, and P3, and brains were analyzed at 6~8 weeks of age. For retinal AVM analysis in endothelial-specific *Alk1*-iKO (*Scl*CreER;*Alk1*$^{2f/2f}$; *Alk1*-iKO^{EC}) mice, tamoxifen (75 μg/g bw) was administered intragastrically once at P4, and retinas were harvested at P6. Tamoxifen-injected CreER-negative littermates served as controls. All animal procedures were conducted in accordance with the NIH Guide for the Care and Use of Laboratory Animals and were approved by the Institutional Animal Care and Use Committee of the Barrow Neurological Institute.

Skin wound generation and blue latex dye injection

Adult male and female mice (6−8 weeks old) were anesthetized in an induction chamber with 4% isoflurane and maintained under 2% isoflurane. A 3 mm biopsy punch was used to generate a wound on the mid-dorsum, and Betadine was applied to the wound site. On Day 8, mice were anesthetized with ketamine/xylazine (0.1 mg/0.015 mg/g bw, i.p.) and perfused sequentially with 10 ml of vasodilator solution (10 U/ml heparin, 0.04 mg/ml papaverine, and 100 μM sodium nitroprusside) followed by 10% formalin. Blue latex dye (5 μl/g bw; VWR, 470024-612) was injected into the left ventricle after clipping the descending aorta. Mice were briefly rinsed with PBS and the back hair was removed by depilatory cream. Dorsal skin tissues were post-fixed in 10% formalin overnight, dehydrated in graded methanol (25−100%), and cleared in benzyl alcohol:benzyl benzoate (1:1; Fisher, AC148390010, AC105860010). Vascular images were captured using a stereo microscope equipped with a CCD camera (Leica) and vessel density was quantified by ImageJ.

Collateral vessel density measurement

Adult mice were perfused with vasodilator, formalin, and blue latex dye as described above. Brains were harvested, and the number of pial collateral vessels – defined as arteriole-to-arteriole

anastomoses connecting the middle cerebral artery (MCA), anterior cerebral artery (ACA), and posterior cerebral artery (PCA) – was counted in each hemisphere. In adult dorsal skin, collateral anastomoses between two lateral thoracic arteries were counted after hair removal. In neonatal dorsal skin, arteries were visualized by whole-mount immunostaining with anti-SMA-Cy3 antibody, and collateral connections were quantified using the same method as in adults.

Quantification of latex-injected vessel volume in brain

Latex-injected, cleared brains were sectioned using a 1 mm coronal mouse brain slicer (Zivic Instruments), and all slices were imaged using the z-stack function of a fluorescence microscope (Keyence, BZ-X800). Total latex-filled vessels and AVM volumes were quantified using the 3D cell count function of the BZ-X800 Analyzer software (Keyence).

Whole-mount immunostaining

Skin tissues were fixed in 4% paraformaldehyde at room temperature for 1 h, washed with PBS, and permeabilized overnight at 4°C in blocking buffer (1% BSA, 0.01% Sodium deoxycholate, 0.3% Triton X-100 in PBS, pH 7.4). Samples were incubated overnight at 4°C with anti-SMA-Cy3 (Sigma, C6198) diluted in blocking buffer. After washing with PBST (0.25% Triton X-100 in PBS), tissues were incubated with appropriate fluorescence-conjugated secondary antibodies (Invitrogen) for 2 h at room temperature, dehydrated in graded methanol, and cleared in benzyl alcohol:benzyl benzoate (1:1). Fluorescent images were acquired using a Keyence BZ-X710 microscope.

Immunofluorescence

Eyeballs were collected from neonatal pups and fixed in 4% paraformaldehyde for 50 min at room temperature. Retinas were dissected and blocked for 1 h in blocking buffer (0.25% Triton X-100, 0.01% Na-deoxycholate, 3% BSA in PBS, pH 7.4). Samples were incubated overnight at 4 °C with the following primary antibodies: anti-CD31 (Biocare medical, CM303B) and anti-phospho-VEGFR2 (Tyr1175; Cell signaling, 2478). After five washes with PBST, retinas were incubated with appropriate fluorescence-conjugated secondary antibodies (Invitrogen) for 2 h at room temperature, washed again, and mounted with ProLong™ Gold Antifade Mountant (Invitrogen, P36930). Images were acquired using a Keyence BZ-X710 fluorescence microscope.

Hemoglobin level

Blood samples were collected by tail amputation, and hemoglobin levels were measured using a hemoglobin photometer (Stanbio Laboratory, Hemopoint H2).

Statistical analysis

Data are expressed as mean ± standard deviation (SD). Data normality was assessed using Shapiro-Wilk or Kolmogorov-Smirnov test. For normally distributed data, two-group comparisons used an unpaired two-tailed Student's *t*-test; comparisons among multiple groups used one-way or two-

way ANOVA followed by Tukey's or Sidak's post hoc test, respectively. For non-normally distributed data, Kruskal-Wallis test followed by Dunn's post hoc test was used. Lesion category frequencies were compared by Fisher's exact test. For correlation analyses, Pearson correlation coefficients and simple linear regression with 95% confidence intervals for the slope were computed. $P < 0.05$ was considered significant. Statistical analyses were performed using Prism 9.4 (GraphPad). ns, not significant; *, $P < 0.05$; **, $P < 0.01$; ***, $P < 0.001$; ****, $P < 0.0001$.

Results

Rabep2 loss reduces collateral density and ameliorates brain AVM severity

To test whether collateral density influences AVM severity, we combined the *Scl*CreER;*Eng*$^{2f/2f}$ (*Eng*-iKO^{EC}) brain AVM model with *Rabep2*-knockout mice. Existing brain AVM mouse models are limited by high mortality from severe intracranial and visceral AVM-related hemorrhages and by variability from procedural technique [14–17]. The *Eng*-iKO^{EC} model reliably produces brain AVMs in adult mice with ~90% incidence; at 6–8 weeks collateral density has already stabilized, making this model suitable for dissecting collateral-AVM relationships [18].

Endothelial *Eng* deletion was induced at P1-P3 in four groups: *Eng*$^{2f/2f}$ (Control), *Eng*$^{2f/2f}$;*Rabep2*$^{-/-}$ (*Rabep2*-KO), *Scl*CreER;*Eng*$^{2f/2f}$ (*Eng*-iKO^{EC}), and *Scl*CreER;*Eng*$^{2f/2f}$;*Rabep2*$^{-/-}$ (*Eng/Rabep2*-dKO^{EC}). At 6–8 weeks, latex perfusion was used to visualize collateral arteries and AVM lesions. Consistent with previous reports [7, 8], *Rabep2*-KO brains showed a marked reduction in pial collateral connections among MCA-ACA-PCA territories, down to ~25% of control levels (Fig. 1a, b, e). In *Eng*-iKO^{EC} and *Eng/Rabep2*-dKO^{EC} brains, collateral counts in non-AVM regions reproduced this difference, indicating that *Rabep2* loss reduces collateral density irrespective of AVM presence (Fig. 1c–e).

Control and *Rabep2*-KO mice showed no vascular abnormalities (Fig. 2a, b), whereas *Eng*-iKO^{EC} and *Eng/Rabep2*-dKO^{EC} brains developed dilated, tortuous vessels characteristic of AVM (Fig. 2c, d). Lesions were scored as no AVM, arteriovenous fistula (AVF), or nidal AVM (a tangled vascular nidus with dilated veins) (Fig. 2e). About 90% of *Eng*-iKO^{EC} animals developed AVM (~80%) or AVF (~10%), whereas in *Eng/Rabep2*-dKO^{EC} mice showed mostly AVF (~70%) with only ~20% showed nidal AVM (Fig. 2c–e). Consistently, *Eng*-iKO^{EC} mice showed reduced hemoglobin levels, whereas *Eng/Rabep2*-dKO^{EC} mice maintained control-like levels (Fig. 2f).

Latex-filled vessel volume across serial sections was increased ~3-fold in *Eng*-iKO^{EC} brains compared to controls, whereas *Eng/Rabep2*-dKO^{EC} brains were comparable to control (Fig. 2g, i). Collateral number correlated positively with latex-injected vessel volume (Fig. 2h; R = 0.8552; R-squared = 0.7313; $P = 0.0142$). The two genotypes occupied non-overlapping ranges of collateral number (Fig. 1e) and formed two separated clusters. This analysis is therefore not intended to define a quantitative dose-response. Rather, it shows that animals with fewer collaterals had lower vessel volume, supporting the hypothesis that reduced collateral density is associated with decreased AVM severity in the brain.

Collateral density positively correlates with AVM severity in dorsal skin

Strain-dependent differences in collateral density are consistent across pial, coronary, intestinal, and hindlimb circulations in adults [1, 2, 6], and pial collateral density declines from P1 to P21 before stabilizing [2]. To our knowledge, collateral remodeling between the lateral thoracic arteries of dorsal skin has not been described; we observed a comparable developmental decline, stabilizing at 9–11 connections in adult control mice (Supplemental Fig. 1a, b), whereas *Rabep2*-KO mice retained fewer than 5 connections (Supplemental Fig. 1c, d).

To test the impact on skin AVM formation, we induced global *Alk1* deletion in four adult groups: $R26^{+/+}$;$Alk1^{2f/2f}$ (Control), $R26^{+/+}$;$Alk1^{2f/2f}$;$Rabep2^{-/-}$ (*Rabep2*-KO), $R26^{CreER/+}$;$Alk1^{2f/2f}$ (*Alk1*-iKO), and $R26^{CreER/+}$;$Alk1^{2f/2f}$;$Rabep2^{-/-}$ (*Alk1/Rabep2*-dKO). *Rabep2*-KO and *Alk1/Rabep2*-dKO mice had ~60% fewer collaterals than control and *Alk1*-iKO mice (Fig. 3a–d, f).

At the wound site, control and *Rabep2*-KO mice showed normal arterial labeling without AVM (Fig. 3a, b). *Alk1*-iKO mice developed skin AVMs with 100% penetrance (Fig. 3c), whereas *Alk1/Rabep2*-dKO mice showed a more variable and generally attenuated AVM phenotype (Fig. 3d) with a ~40% reduction in latex-perfused vascular density (Fig. 3e, g). Collateral number again correlated with AVM severity across individual animals (Fig. 3h), and the hemoglobin decline from Day 0 to Day 8 was blunted in *Alk1/Rabep2*-dKO compared with *Alk1*-iKO mice (Fig. 3i).

Retinal AVM formation is unaffected by *Rabep2* deletion

Because *Rabep2* also regulates VEGFR2 trafficking and expression [9], its loss could affect AVM formation independently of collaterals. To test this, we used the retina, a vascular bed that lacks native collateral arterioles [1]. Endothelial *Alk1* deletion was induced on *Rabep2* wildtype and knockout backgrounds, and retinas were whole-mounted and stained for CD31.

Alk1-iKO^{EC} and *Alk1/Rabep2*-dKO^{EC} retinas developed AVMs at comparable numbers (Fig. 4a–e), and phospho-VEGFR2 immunoreactivity, used as a qualitative readout of local VEGFR2 activation, appeared similarly elevated at AVM lesions in both genotypes (Fig. 4c, d). These findings indicate that the attenuated AVM severity in brain and skin of *Rabep2*-KO mice reflects reduced collateral density rather than impaired VEGFR2 signaling.

Discussion

Our results identify collateral vessel density as a host-specific modifier of AVM severity. *Rabep2*-deficient mice, which have a sparse native collateral network, developed attenuated AVMs in both *Eng*- and *Alk1*-inducible knockout models. Across individual animals, lower collateral numbers were correlated with small lesion volume, milder morphology, and preserved hemoglobin levels. Two observations provide no support for a collateral-independent, VEGFR2-mediated action of *Rabep2*: *Rabep2* deletion did not affect AVM formation in the retina, a vascular bed that lacks native collaterals; and pVEGFR2 immunoreactivity at AVM lesions was comparable between genotypes (Fig. 4c, d).

These data argue against the view that collaterals are uniformly protective. Under ischemia, collaterals preserve perfusion; at an arteriovenous shunt, additional arterial input instead lowers the input resistance of the lesion and channel more flow into the nidus, consistent with the network models in which intermediate anastomoses substantially increase collateral supply [19, 20]. Because elevated flow itself drives arteriogenesis [21], abundant collaterals may sustain a self-reinforcing cycle of shunt flow, venous hypertension, and rupture risk, and may ultimately be incorporated into the lesion circuit. Direct flow measurements will be required to test this.

Within each vascular bed, lesion burden correlated with collateral number across individual animals. In skin, where incomplete collateral suppression allowed animals to span a continuous range of collateral numbers, latex-perfused vascular density scaled with collateral number across that range ($R^2 = 0.7888$, $P < 0.0001$; Fig. 3h). In brain, latex-perfused lesion volume likewise correlated with collateral number ($R^2 = 0.7313$, $P = 0.0142$; Fig. 2h), although collateral number fell into two non-overlapping clusters, one for each genotype, reflecting the major-effect nature of *Rabep2* at the *Canq1* locus: deletion reduces pial collateral number to ~25% of control [7, 8], so intermediate collateral states are not accessible with this allele. The two beds were quantified on different measures, and the relationships are therefore described separately; what they share is that animals with fewer collaterals developed less severe AVM lesions. Grading collateral density within a single genetic background– for example using hypomorphic alleles that confer intermediate collateral number [7]–would allow the relationship in brain to be characterized as fully as in skin. The principal limitations are the small group sizes available for volumetric correlation, which establish the direction of the relationship but constrain the precision of the slope estimate.

Collateral vessel density therefore acts as a physiological modulator of AVM severity, providing a mechanistic link between vascular architecture and disease outcome. As proof of concept, this suggests that collateral status may predict lesion severity, and that modulating flow distribution around an established nidus could complement gene-targeted and surgical strategies aimed at the nidus itself to reduce lesion progression and rupture risk.

Acknowledgements
We thank Dr. Helen Arthur (Newcastle University, UK) for providing *Eng*-floxed mice, and Kellie Kim (University of Southern California) for technical assistance.

Author contributions
HC designed and performed experiments, analyzed the data, and wrote the first draft; HKL and DAM provided *Rabep2*-knockout mice and contributed to data analysis. SPO designed and supervised the project. All authors reviewed and approved the manuscript.

Funding
This work was supported by the US Department of Defense (PR161205), the Leducq Foundation (ATTRACT), and Barrow Neurological Foundation to SPO; and by Barrow Neurological Foundation Postdoctoral Fellowship to HC.

Disclosures
The authors have declared that no conflict of interest exists.

References

1. Faber JE, Chilian WM, Deindl E, et al (2014) A Brief Etymology of the Collateral Circulation. ATVB 34:1854–1859. https://doi.org/10.1161/ATVBAHA.114.303929

2. Chalothorn D, Faber JE (2010) Formation and maturation of the native cerebral collateral circulation. J Mol Cell Cardiol 49:251–259. https://doi.org/10.1016/j.yjmcc.2010.03.014

3. Billinger M, Kloos P, Eberli FR, et al (2002) Physiologically assessed coronary collateral flow and adverse cardiac ischemic events: a follow-up study in 403 patients with coronary artery disease. Journal of the American College of Cardiology 40:1545–1550. https://doi.org/10.1016/S0735-1097(02)02378-1

4. Lohr NL (2014) Collateral Development: The Quest Continues. Circ Res 114:591–593. https://doi.org/10.1161/CIRCRESAHA.114.303402

5. Lee HK, Widmayer SJ, Huang M-N, et al (2019) Novel Neuroprotective Loci Modulating Ischemic Stroke Volume in Wild-Derived Inbred Mouse Strains. Genetics 213:1079–1092. https://doi.org/10.1534/genetics.119.302555

6. Chalothorn D, Clayton JA, Zhang H, et al (2007) Collateral density, remodeling, and VEGF-A expression differ widely between mouse strains. Physiological Genomics 30:179–191. https://doi.org/10.1152/physiolgenomics.00047.2007

7. Lucitti JL, Sealock R, Buckley BK, et al (2016) Variants of Rab GTPase–Effector Binding Protein-2 Cause Variation in the Collateral Circulation and Severity of Stroke. Stroke 47:3022–3031. https://doi.org/10.1161/STROKEAHA.116.014160

8. Lee HK, Kwon DH, Aylor DL, Marchuk DA (2022) A cross-species approach using an in vivo evaluation platform in mice demonstrates that sequence variation in human RABEP2 modulates ischemic stroke outcomes. American Journal of Human Genetics 109:1814–1827. https://doi.org/10.1016/j.ajhg.2022.09.003

9. Kofler N, Corti F, Rivera-Molina F, et al (2018) The Rab-effector protein RABEP2 regulates endosomal trafficking to mediate vascular endothelial growth factor receptor-2 (VEGFR2)-dependent signaling. J Biol Chem 293:4805–4817. https://doi.org/10.1074/jbc.M117.812172

10. Ventura A, Kirsch DG, McLaughlin ME, et al (2007) Restoration of p53 function leads to tumour regression in vivo. Nature 445:661–665. https://doi.org/10.1038/nature05541

11. Göthert JR, Gustin SE, Van Eekelen JAM, et al (2004) Genetically tagging endothelial cells in vivo: bone marrow-derived cells do not contribute to tumor endothelium. Blood 104:1769–1777. https://doi.org/10.1182/blood-2003-11-3952

12. Park SO, Lee YJ, Seki T, et al (2008) ALK5- and TGFBR2-independent role of ALK1 in the pathogenesis of hereditary hemorrhagic telangiectasia type 2. Blood 111:633–642. https://doi.org/10.1182/blood-2007-08-107359

13. Mahmoud M, Allinson KR, Zhai Z, et al (2010) Pathogenesis of Arteriovenous Malformations in the Absence of Endoglin. Circulation Research 106:1425–1433. https://doi.org/10.1161/CIRCRESAHA.109.211037

14. Choi E-J, Chen W, Jun K, et al (2014) Novel Brain Arteriovenous Malformation Mouse Models for Type 1 Hereditary Hemorrhagic Telangiectasia. PLoS ONE 9:e88511. https://doi.org/10.1371/journal.pone.0088511

15. Park SO, Wankhede M, Lee YJ, et al (2009) Real-time imaging of de novo arteriovenous malformation in a mouse model of hereditary hemorrhagic telangiectasia. J Clin Invest 119:3487–3496 https://doi.org/10.1172/JCI39482

16. Milton I, Ouyang D, Allen CJ, et al (2012) Age-Dependent Lethality in Novel Transgenic Mouse Models of Central Nervous System Arteriovenous Malformations. Stroke 43:1432–1435. https://doi.org/10.1161/STROKEAHA.111.647024

17. Scherschinski L, Han C, Kim YH, et al (2023) Localized conditional induction of brain arteriovenous malformations in a mouse model of hereditary hemorrhagic telangiectasia. Angiogenesis 26:493–503. https://doi.org/10.1007/s10456-023-09881-w

18. Han C, Nguyen CL, Scherschinski L, et al (2023) VEGFR2 Expression Correlates with Postnatal Development of Brain Arteriovenous Malformations in a Mouse Model of Type I Hereditary Hemorrhagic Telangiectasia. Biomedicines 11:3153. https://doi.org/10.3390/biomedicines11123153

19. Otani T, Nishimura N, Yamashita H, et al (2023) Computational modeling of multiscale collateral blood supply in a whole-brain-scale arterial network. PLoS Comput Biol 19:e1011452. https://doi.org/10.1371/journal.pcbi.1011452

20. Padmos RM, Terreros NA, Józsa TI, et al (2021) Modelling the leptomeningeal collateral circulation during acute ischaemic stroke. Medical Engineering & Physics 91:1–11. https://doi.org/10.1016/j.medengphy.2021.03.003

21. Heil M, Schaper W (2004) Influence of Mechanical, Cellular, and Molecular Factors on Collateral Artery Growth (Arteriogenesis). Circulation Research 95:449–458. https://doi.org/10.1161/01.RES.0000141145.78900.44

Figure legends

Fig. 1 *Rabep2* deletion reduces pial collateral density in control and *Eng*-iKO^{EC} brains.
a–d, Representative images of latex dye-injected cerebrovasculature in control (a, n = 23 brains), *Rabep2*-KO (b, n = 14), *Eng*-iKO^{EC} (c, n = 6), and *Eng*/*Rabep2*-dKO^{EC} (d, n = 10) mice at 6–8 weeks (*left*). Magnified views of the boxed regions (*right*) show collateral arterial connections between ACA-MCA, MCA-PCA, and ACA-PCA territories (red dots). Scale bars, 1 mm. **e,** Quantification of collateral density per hemisphere in each genotype. Data are mean ± SD. One-way ANOVA with Tukey's post hoc test.

Fig. 2 *Rabep2* deletion reduces AVM severity and associated vascular phenotypes in the *Eng*-iKO^{EC} brain AVM model.
a–d, Representative latex dye-injected brain images from control (a), *Rabep2*-KO (b), *Eng*-iKO^{EC} (c), and *Eng*/*Rabep2*-dKO^{EC} (d) mice (*upper panels*). Enlarged views of the boxed regions (*middle and lower panels*) highlight AVMs (white arrows), an AV shunt (black arrow), and an AVM in the hippocampal region (arrowhead). Scale bars, 1 mm. **e,** Quantification of AVM incidence across genotypes (n = 10 brains per group). Nidus-type AVMs were scored as AVM and small AV fistulas as AVF. Fisher's exact test comparing the proportion of nidal AVM between *Eng*-iKO^{EC} and *Eng*/*Rabep2*-dKO^{EC}. P = 0.0142. **f,** Systemic hemoglobin levels in each group (n = 8–18 mice). **g,** Quantification of latex-filled vessel volume (n = 3–7 brains per group). **h,** Correlation between total latex-filled vessel volume and the number of collateral arterial connections in *Eng*-iKO^{EC} (n = 3) and *Eng*/*Rabep2*-dKO^{EC} (n = 4) brains (Simple linear regression: slope = 2.414 (95% CI 0.73 to 4.09) ; Pearson R = 0.8552, R^2 = 0.7313, P = 0.0142). **i,** Representative serial brain sections used for volume quantification. Scale bars, 1 mm. Data in f and g are mean ± SD. One-way ANOVA with Tukey's post hoc test (f, g)

Fig. 3 AVM severity correlates with collateral vessel density in the *Alk1*-iKO wound-induced skin AVM model.
a–d, Representative latex dye-injected dorsal skin vasculature of control (a), *Rabep2*-KO (b), *Alk1*-iKO (c), and *Alk1*/*Rabep2*-dKO (d) mice. Arrowheads indicate collateral arterial connections; asterisks mark wound sites. Scale bars, 1 mm. **e**, Converted vessel-density images used for quantification. Scale bars, 1 mm. **f,** Quantification of collateral numbers (n = 8–11 mice per group). **g,** Quantification of latex-perfused vascular density (n = 8–10 mice per group). **h,** Correlation between vascular density and collateral number in *Alk1*-iKO (n = 5) and *Alk1*/*Rabep2*-dKO (n = 8) skins. Simple linear regression: slope = 2.270 (95% CI 1.49 to 3.04); Pearson R = 0.8882, R^2 = 0.7888, P < 0.0001. **i,** Hemoglobin levels at Day 0 and Day 8 after wounding (n = 7–12 mice per group). Data in f, g, i are mean ± SD. One-way ANOVA with Tukey's post hoc test (f, g); two-way ANOVA with Sidak's post hoc test (i).

Fig. 4 *Rabep2* deletion does not affect AVM formation in a retinal AVM model lacking arterial collaterals.

a–d, Representative CD31 (top) and phospho-VEGFR2 (bottom) staining of retina flat-mounts from control (a), *Rabep2*-KO (b), *Alk1*-iKO^{EC} (c), and *Alk1*/*Rabep2*-dKO^{EC} (d) mice. a, artery; v, vein; arrows indicate AVMs. Scale bars, 100 μm. **e,** Quantification of AVM number per retina (n = 14–26 retinas per group). Data are mean ± SD. One-way ANOVA with Tukey's post hoc test and Shapiro-Wilk normality test.

Supplemental Fig. 1 *Rabep2* deletion reduces collateral arterial connections in dorsal skin.

a, Developmental time course of collateral formation between lateral thoracic arteries at P1, P7, P21, and 3 months in control mice. Representative SMA-immunostained (P1, P7) and latex dye-injected (P21, 3M) images are shown (*left*), with magnified boxed regions (*right*). White dots indicate collateral arterial connections. Scale bars, 1 mm. **b,** Quantification of collateral number across developmental stages. (n = 3–4 mice per stage) **c,** Representative latex-injected dorsal skin images from control and *Rabep2*-KO mice at 1.5 months (*left*), with magnified boxed regions (*right*). Arrowheads indicate collateral connections. Scale bars, 1 mm. **d,** Quantification of collaterals (n = 7 mice per group). Data in b and d are mean ± SD. One-way ANOVA with Tukey's post hoc test (b); unpaired two-tailed Student's t-test (d).

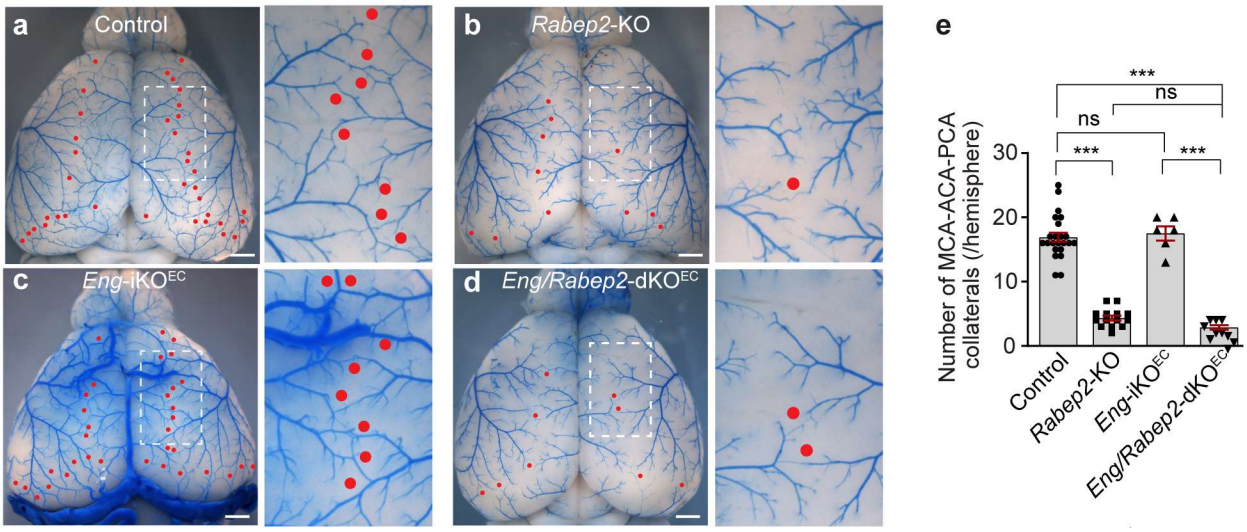

a
Control
b
Rabep2-KO
c
Eng-iKOEC
d
Eng/Rabep2-dKOEC
e
Number of MCA-ACA-PCA collaterals (/hemisphere)
30
20
10
0
***
ns
ns
***
***
Control
Rabep2-KO
Eng-iKOEC
Eng/Rabep2-dKOEC

Figure 1

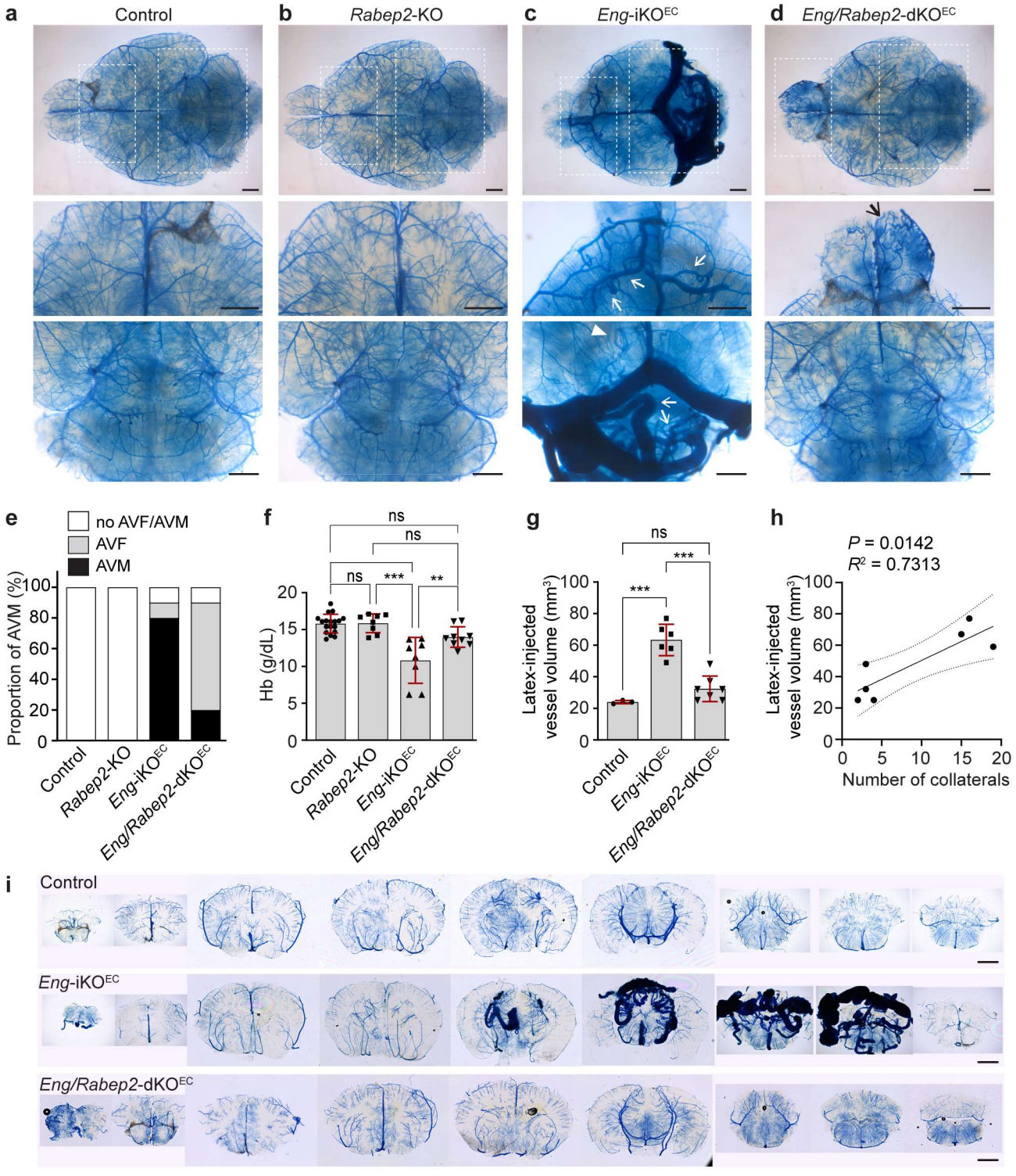

a
Control
b
Rabep2-KO
c
Eng-iKOEC
d
Eng/Rabep2-dKOEC
e
no AVF/AVM
AVF
AVM
Proportion of AVM (%)
Control
Rabep2-KO
Eng-iKOEC
Eng/Rabep2-dKOEC
f
Hb (g/dL)
ns
***
**
g
Latex-injected vessel volume (mm3)
h
P = 0.0142
R2 = 0.7313
Number of collaterals
i
Control
Eng-iKOEC
Eng/Rabep2-dKOEC

Figure 2

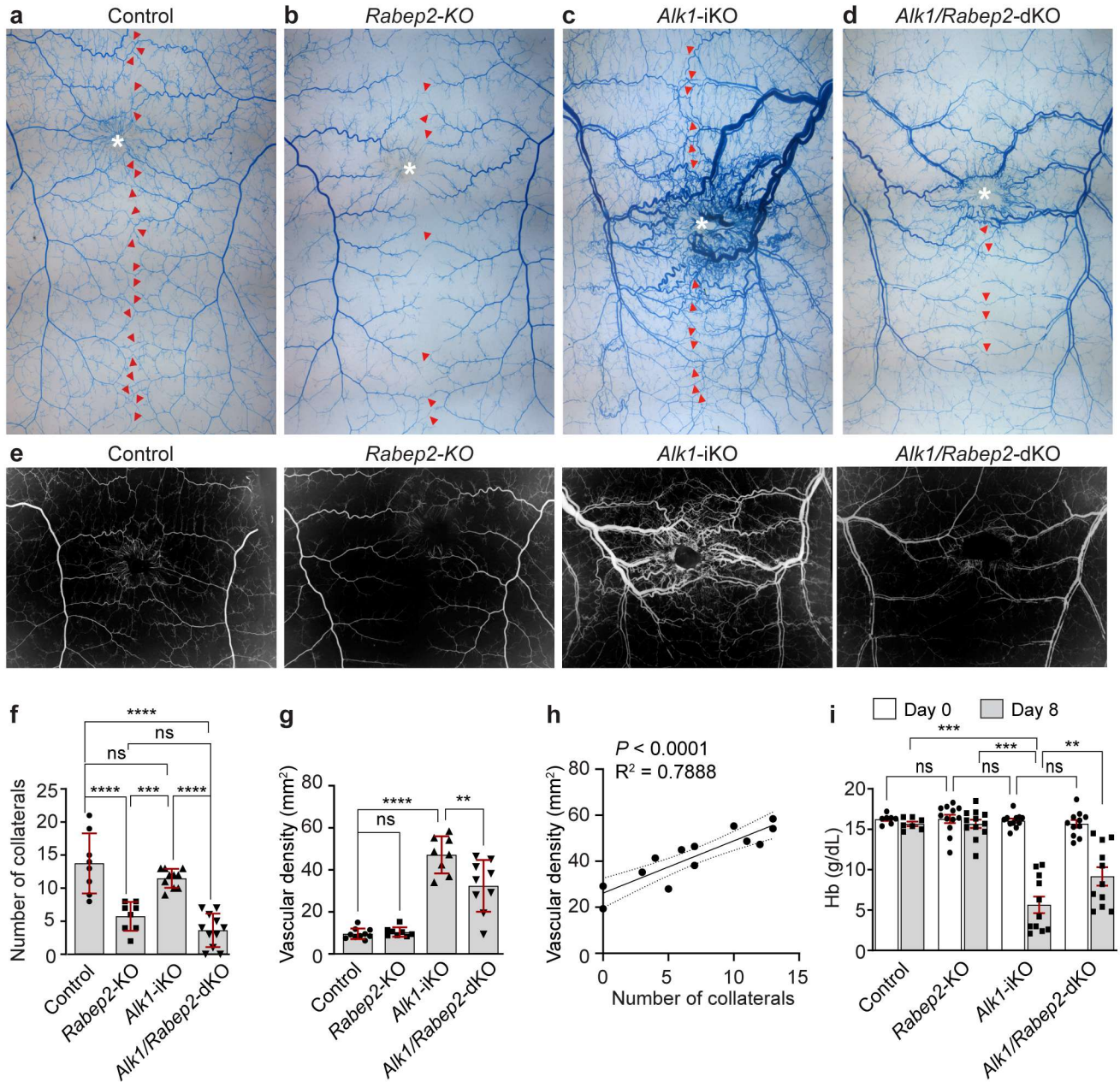

a
Control
b
Rabep2-KO
c
Alk1-iKO
d
Alk1/Rabep2-dKO
e
Control
Rabep2-KO
Alk1-iKO
Alk1/Rabep2-dKO
f
Number of collaterals
****
ns
ns
****
***
****
Control
Rabep2-KO
Alk1-iKO
Alk1/Rabep2-dKO
g
Vascular density (mm²)
****
ns
**
Control
Rabep2-KO
Alk1-iKO
Alk1/Rabep2-dKO
h
P < 0.0001
R² = 0.7888
Vascular density (mm²)
Number of collaterals
i
Day 0
Day 8
***
***
**
ns
ns
ns
Hb (g/dL)
Control
Rabep2-KO
Alk1-iKO
Alk1/Rabep2-dKO

Figure 3

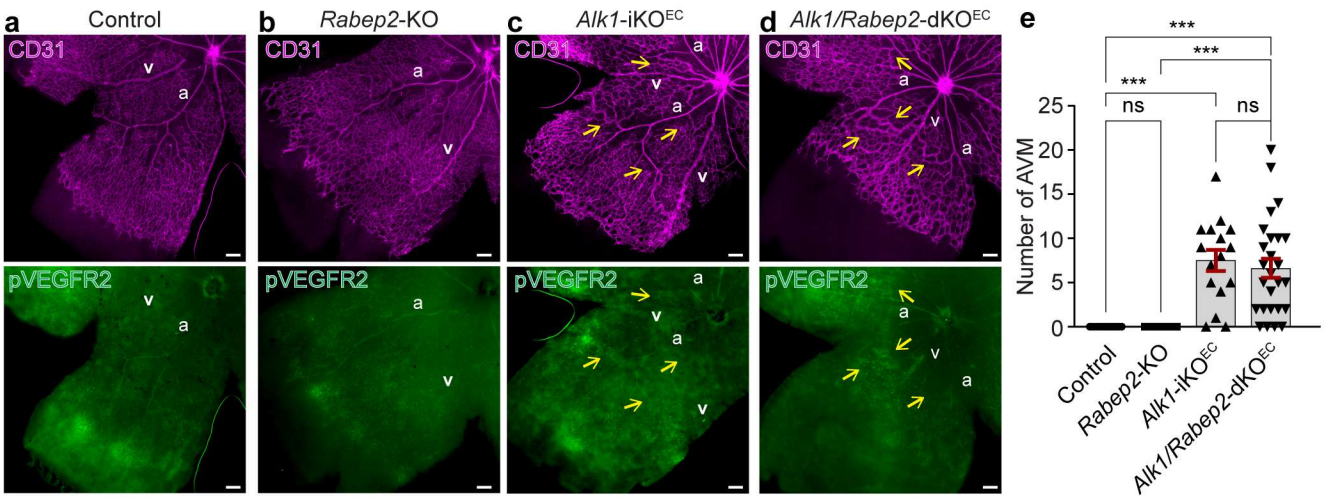

a Control
b Rabep2-KO
c Alk1-iKOEC
d Alk1/Rabep2-dKOEC
e
CD31
pVEGFR2
v
a
***
ns
Number of AVM
25
20
15
10
5
0
Control
Rabep2-KO
Alk1-iKOEC
Alk1/Rabep2-dKOEC

Figure 4

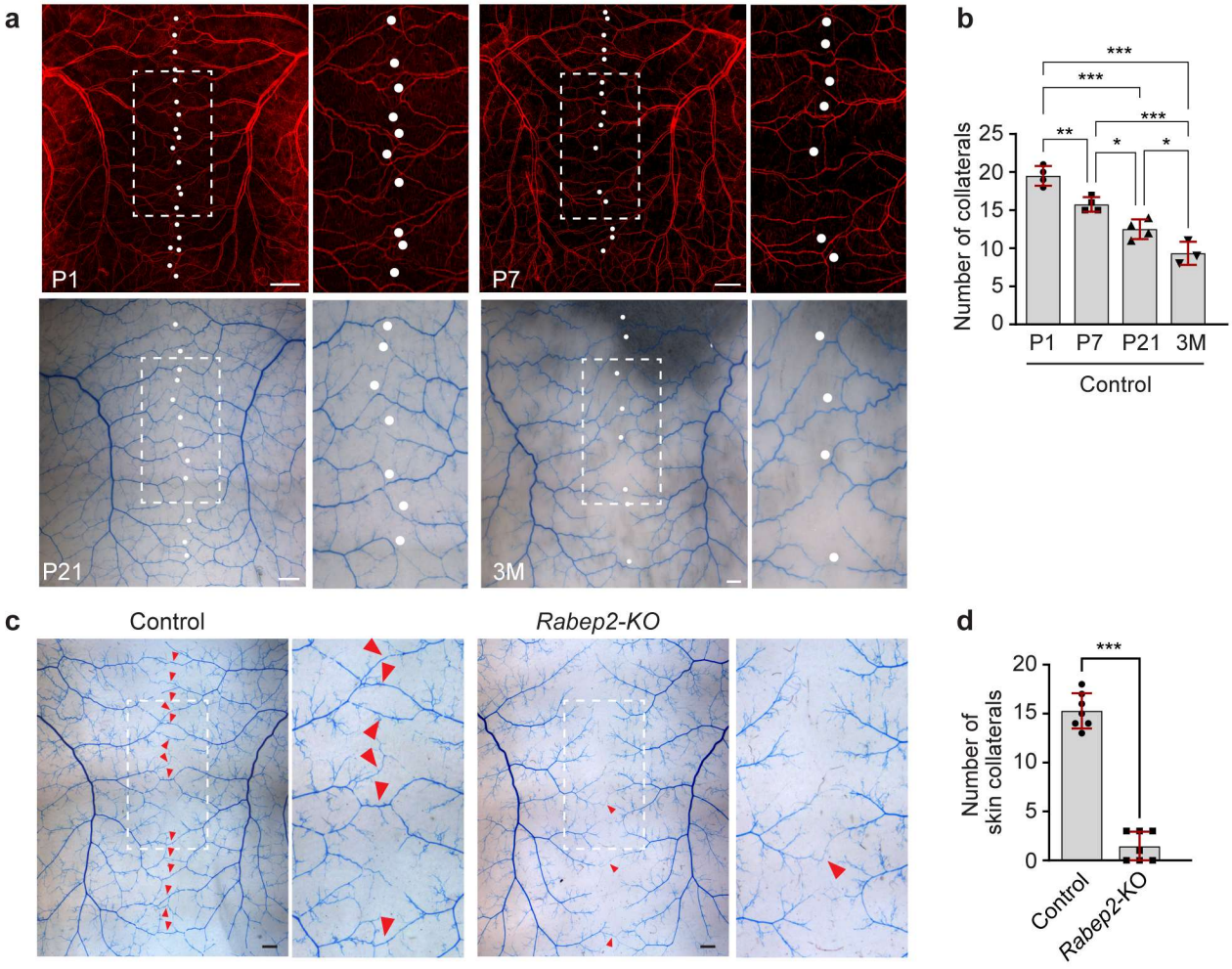

a
P1
P7
P21
3M
b
Number of collaterals
25
20
15
10
5
0
P1
P7
P21
3M
Control
***
***
***
**
*
*
c
Control
Rabep2-KO
d
Number of skin collaterals
20
15
10
5
0
***
Control
Rabep2-KO

Figure S1